

Radiation shielding parameterizations of FeSO_4 , CuSO_4 , NiSO_4 and ZnSO_4 Compounds: using (XRF) technique and Monte Carlo FLUKA approach

M. A. Majeed

Ministry of Education, Iraq.

Received 14 August 2023; accepted 9 January 2024

The mass attenuation coefficient (MAC) for different sulphate compounds can be estimated by using the Energy Dispersive X-ray Fluorescence (EDXRF), also known as X-ray Fluorescence (XRF) technique. The X-ray photons emitted have different energies depending on incident photon energy, atomic weight, and molecular structure of tested material. The excitation energy of the gamma rays source with 59.53 keV was obtained by using ^{241}Am (40 μCi). The (MAC) for sulphate compounds of a different element (Fe, Ni, Cu, Zn) have been calculated by measuring the intensity difference for $k\alpha$ in pure elements and their compounds. The determined results showed that the maximum value for (μm) was in FeSO_4 . These results are consistent with the theoretical value obtained by the XCOM software in addition to investigating the wide energy response of photon interaction with the introduced compounds using the FLUKA Monte Carlo simulation software. The mass attenuation coefficient (MAC) of these compounds is numerically evaluated in the energy range 0.015-15 MeV using the FLAIR code. The computed (μm) is used to generate significant radiation protection factors such as the linear attenuation coefficient (LAC), half-layer value (HVL), effective (Z_{eff}), and equivalent (Z_{eq}) atomic number. For studying the shielding effectiveness and efficiency, for fast and thermal neutron radiation, the removal cross-section $\sum R$ was given.

Keywords: Scanning electronic microscope; X-ray fluorescent; sulphate compounds; mass attenuation coefficient (μm) and FLUKA Monte Carlo approach.

DOI: <https://doi.org/10.31349/RevMexFis.70.040401>

1. Introduction

X-ray photons are created when an inner orbital electron is ejected and when atomic orbital electrons move from high to low energy levels [1,2]. The property of the atomic number dependence of the absorption of X-ray photons was quickly applied for medical diagnostic purposes. After the discovery of X-ray diffraction by Max von Laue in 1913, major fields of materials analysis have developed. XRF spectroscopy isolates narrow energy bands from polychromatic beam characteristic radiation produced in the sample using either the diffracting power of a single crystal or a proportional detector. The first of these methods is called wavelength dispersive spectrometry and the second is energy dispersive spectrometry [3]. The increase in the use of nuclear energy in all branches of human activities has been linked to the production and use of radioactive materials which has led to an increase in danger associated with these activities [4]. To gain a high level of security and be safe from exposure to radiation of all kinds, the radioactive materials in laboratories or in fields must be surrounded by protective shields to avoid the danger caused by these radiations. The shielding materials must meet some requirement, *e.g.* dealing with all kinds and levels of radiation, have a high resistance to the effect of radiation and with low intrinsic radioactivity, in addition to their abundance, easy to be manufactured and cost-effectiveness [5]. The deformation pattern of the crystal will be increased when increasing the relative formation and this leads to an increase in the recrystallization velocity of nuclei growth and the linear velocity of growth as well. If both velocities are

evenly increased when the relative formation increases then the effect of relative formation will vanish. The grain size of re-crystallized will decrease when the relative formation increases, hence we can conclude that; the velocity of recrystallization of nuclei growth will be more greatly increased than the linear velocity of new grain growth [6]. X-ray machines have three principal uses as diagnostic, therapeutic, and non-medical radiographic devices. An X-ray tube is usually housed in a heavy lead casing with an aperture through which the primary, or useful, beam emerges. Typically, the beam passes through metal filters (*e.g.*, Al, Cu) to remove unwanted, less penetrating radiation and is then collimated to reduce its width. The housing, supplied by the manufacturer, must conform to certain specifications to limit the leakage radiation that emerges from it during operation. For diagnostic X-ray tubes, regulations require that manufacturers limit the leakage exposure rate at a distance of 1 m from the tube's target to 0.1 Rh^{-1} when operated continuously at its maximum rated current and potential difference [7]. The production of tomographic images is reconstructed by transforming the X-ray attenuation coefficient distribution in a patient body. The final image is produced as a result of a whole chain of processes and is affected by many factors including the technical parameters of the scanner, the type of projection system, and finally the type of reconstruction algorithm applied [8]. The formation of exciting micro beams (X-ray or ion beams) provided elemental mapping down to the few parts per million concentration regime, enhancing the applicability of the ion beam, and X-ray spectrometry was interesting in measuring MCA for glass systems [9-18]. Recently

have interest in using glass samples of ZrO_2 , CaO , Na_2O , P_2O_5 , B_2O_3 , and Bi_2O_3 , oxides was within the goal of many to test of these compounds in terms of shielding against nuclear radiation [19,20]. Other researchers used the Monte Carlo simulation (MC) technique is an effective method to simulate particle transport and interactions with matter and to generate the mechanical and radiation parameters for different shielding materials [21]. Used different sulphate compounds with $AlSO_4$, $BaSO_4$, $KAlSO_4$, and Na_2SO_4 to study the radiation shielding behavior of such materials [22]. Devoted his interest in nano-materials and the extent to which these materials repel radiation especially neutrons [23]. Applied gamma spectroscopy using HPGe detector for photon attenuation measurements [24]. In this work, FLUKA version 4 – 3.0 and Flair GUI were used to estimate the photon radiation coefficients for a group of sulfuric materials such as $FeSO_4$, $CuSO_4$, $NiSO_4$ and $ZnSO_4$. Shielding efficiency and quality were also given. Results for low-energy photon regions will be confirmed with the experimental one.

2. Theoretical framework of radiation shielding parameter calculations

Photon attenuation coefficient μ , describes the attenuation rate that accounts for the total number of atoms in a cm^3 volume of material and the possibility of X-rays or gamma rays being scattered or absorbed from the nucleus or an electron of a material. Table I shows all the mathematical relationships, the Photon attenuation coefficient μ , mass attenuation

TABLE I. Definition of (MAC), (HVL), (TVL) and (MFP).

Formula	Definitions	Units
$\mu = \ln \frac{I_0/I}{x}$	$(I_0 \& I)$ are the incident and transmitted photon intensities respectively and x is the glass thickness	cm^{-1}
$MAC = \mu/\rho$	(MAC) is used for calculating the penetration of photons in shielding materials (ρ) is the shielding material density (g/cm^3)	cm^2/g
$HVL = \ln 2/\mu$	(HVL) is the sample thickness required to reduce the radiation intensity to half of its primary value	cm
$TVL = \ln 10/\mu$	(TVL) is the sample thickness required to reduce the radiation intensity to the tenth of its primary value	cm
$MFP = 1/\mu$	(MFP) is the mean distance traveled by a photon inside a shielding material prior to encountering an interaction	cm

coefficient (MAC), half value layer (HVL), tenth value layer (TVL) and mean free path (MFP) for the attenuation of photons. These characteristic values are often calculated to show the shielding properties quality of any material against X-rays or gamma rays.

3. FLUKA Simulations

FLUKA is a general-purpose Monte Carlo (MC) package. It has many applications for the interaction and transport of nucleons and photons. It uses the best mathematical models and a precision, microscopic approach [25]. FLUKA has a wide range of applications, design shielding, radiation protection, dosimetry, and radiation detector simulation. The 2021.2.9 latest version of FLUKA was published in January 13th, 2023 which was requested and downloaded from the FLUKA site. FLUKA needs a helper code called Flair. Flair is a user-friendly interface for FLUKA code to simplify the editing of FLUKA input cards, running FLUKA, and visualization of the output results. It is fully based on Python language. A Powerful and user-friendly graphical interface For FLUKA is the FLAIR code [24,25]. The latest FLAIR-2.3-0c version was published in 24th-Mar-2023 and can be requested and downloaded from flair site. In this work simulation was done using the following FLUKA and flair parameters:

- The beam profile is assumed to be rectangular and the beam is directed in the positive z-direction.
- GEOBEGIN card: combinational geometry is used in free format.
- for BLKBODY and Void a sphere is defined with $R = 100000$ and $R = 10000$ respectively.
- Right Circular Cylinder code RCC declared for target with $HZ=0.1$ and $R = 5.0$.
- The MGDRAW.F general event subroutine interface was activated by the USERDUMP card
- The VOID region: ASSIGNMA VACUUM VOID.
- EMFCUT production in a material is set equal to the lowest transport cutoffs in the requested region with the introduced material.
- The $35B_2O_3$, $25SiO_2$, $40CaO$, $XSnO_2$ samples have been described using the built-in MATERIAL and COMPOUND cards using B, O, Si, Ca, and Sn elements. All elements except boron are predefined in the FLUKA default library. Boron is defined by a MATERIAL card and its correspondence neutron library was requested by a featured card.
- Simulation was done for 106 primary particles and the code was run for 5 cycles. The results were directed to the output binary files of USRBIN and USRBDX. The

TABLE II. Elemental composition and densities for the introduced samples.

Sample	Compounds	Elements	Elemental weight (%)	Density g/cm^3 This work	Density g/cm^3 Theoretical
S1	FeSO_4	Fe	0.367631	3.72	3.65
		S	0.211085		
		O	0.421285		
S2	CuSO_4	Cu	0.398134	3.64	3.60
		S	0.200903		
		O	0.400963		
S3	NiSO_4	Ni	0.379261	3.92	4.01
		S	0.207202		
		O	0.413536		
S4	ZnSO_4	Zn	0.405008	3.56	3.54
		S	0.198608		
		O	0.396383		

average and mean values were calculated using the FLAIR RUN mode. Figure 1 shows the used simulated geometry.

Experimental analysis

The high purity (99.99%) powder of sulphate compounds (FeSO_4 , CuSO_4 , NiSO_4 , and ZnSO_4) has been obtained from Sigma Aldrich company. Table II gives the elemental composition of these compounds and their measured densities. The mass attenuation coefficients have been determined by measuring of X-rays emitted through a sample compound of known thickness. The experimental arrangement is shown in Fig. 1. The sample compounds have been irradiated with (59.53 keV) X-rays obtained from the ^{241}Am (40 μCi) annular source. The emitted K-line X-ray fluorescents have been collimated by the lead collimator shielded with aluminum and iron to fall on samples, this sample compound was placed in a circular ring having various thicknesses (0.25 – 1.8 mg/cm^2). The X-rays fluorescent has been recorded with the help of a silicon drift detector (SDD) connected to the fast COMTECH multichannel analyzer card. The distance be-

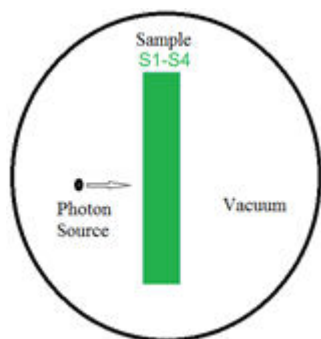


FIGURE 1. The simulation set up for FLUKA code.

tween source to sample is (15 mm) the same as the distance between the sample to the detector with an angle (90°) as shown in Fig. 1.

Results and discussions

Figures 2-5 show the (XRF) measurements for pure elements (Fe, Cu, Ni, Zn) and sulphate compounds respectively. These figures clearly indicate that $k\alpha$ of X-ray energy peaks for pure elements with higher intensity. It has been observed that for compound samples intensity of these $k\alpha$ of X-ray energy peaks was decreased, due to the decreased fraction of elements (Fe, Cu, Ni, Zn) in sulphate compounds. These have been shown in Figs. 3-6 respectively.

Because of the grain form and crystal structure of atoms, the mass attenuation coefficient (MCA) for sulphate compounds was calculated using Table I. It was determined that the (MCA) for sulphate compounds increased with larger molar mass except for Iron sulphate. It can be seen in Fig. 7 and Table III.

The Fig. 8 shows SEM image which is composed of uniformly distributed uneven granular structure.

TABLE III. Calculated experimental and theoretical FLUKA mass attenuation coefficient (MCA) for sulphate compounds.

Samples	MCA	MCA	Percentage Error
	Experimental	Theoretical	
FeSO_4	88.2	87.52	0.007
NiSO_4	44.5	43.20	0.030
CuSO_4	45.23	44.60	0.016
ZnSO_4	46.1	45.20	0.019

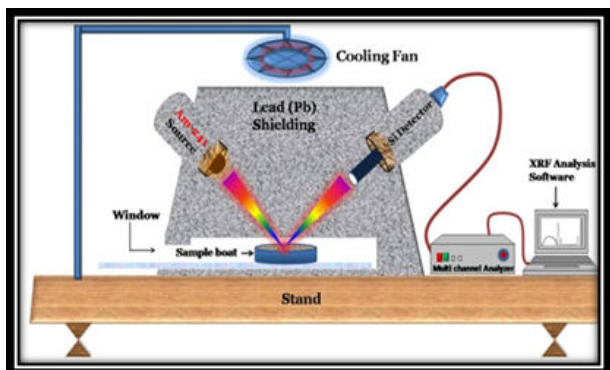


FIGURE 2. The Experimental Set-up.

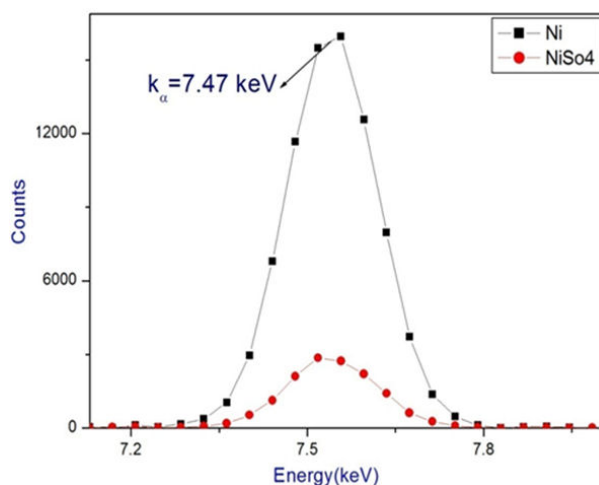


FIGURE 5. Shows the X-ray fluorescence plots for Nickel sulphate.

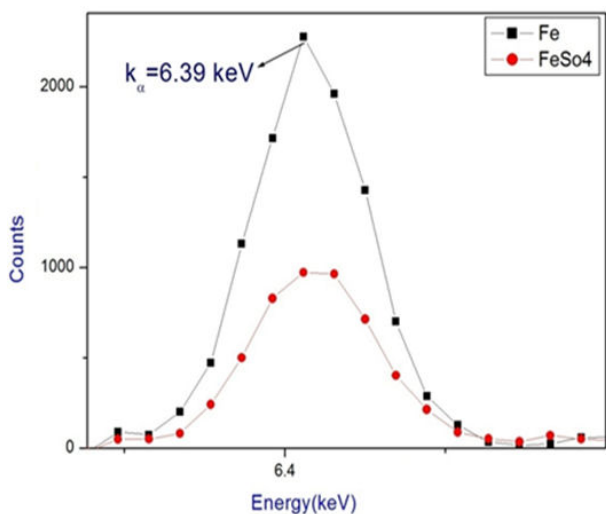


FIGURE 3. Shows the X-ray fluorescence plots for Iron sulphate.

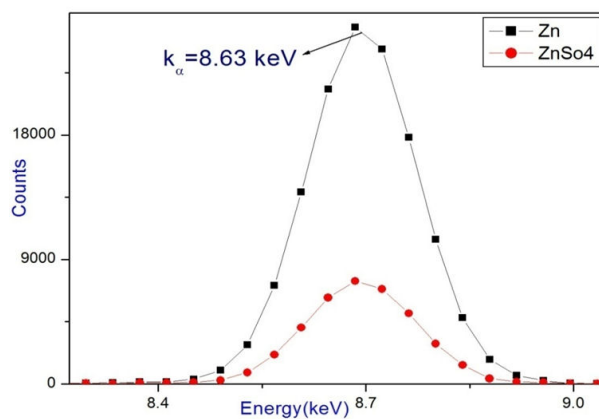


FIGURE 6. Shows the X-ray fluorescence plots for Zinc sulphate.

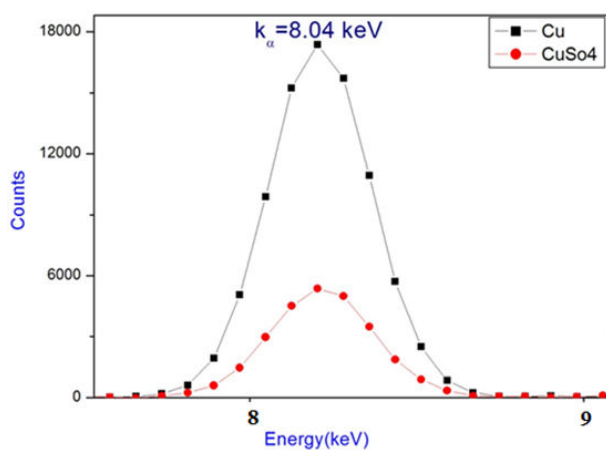


FIGURE 4. Shows the X-ray fluorescence plots for Copper sulphate.

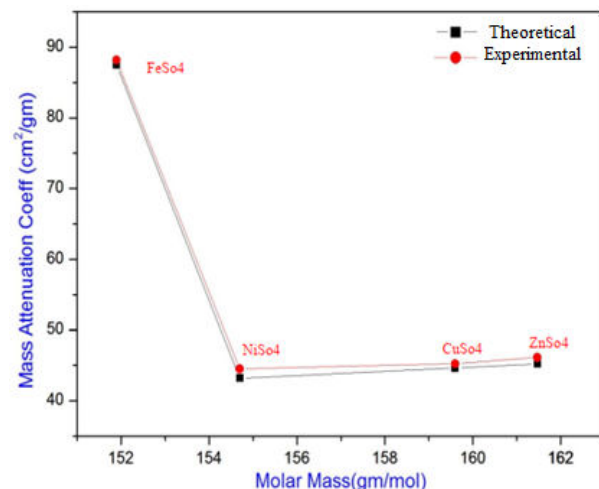


FIGURE 7. The Experimental and theoretical plot between mass attenuation coefficient (MCA) and molar mass of sulphate compounds

Results of Monte Carlo FLUKA simulation

Figure 9 represents the MCA calculated for the (0.0001 - 100 MeV) photon energy range. The right figure is the zoom part for the (0.0001 - 0.01 MeV) low energy. It should be

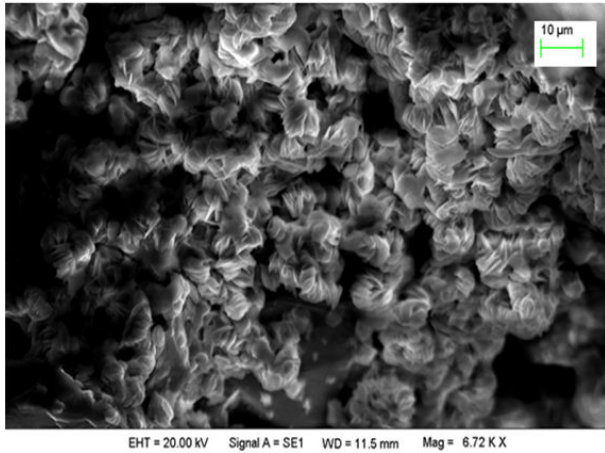


FIGURE 8. The SEM Image For FeSO_4

mentioned that the lower part has 5 peaks at energies 0.0002, 0.0005, 0.001, 0.0024, and 0.009 MeV. The compound FeSO_4 precedes all at 0.001 MeV photon energy. For the energy range from about 0.04 up to 0.1 MeV one can find

ZnSO_4 can have the highest value while the FeSO_4 has the lower values. Based on the MCA calculations, we generate the HVL and The TVL values according to Table I. Results are summarized in Fig. 10. Results show that for about 600 keV the HVL has a value less than (1 cm). As the photon energy increases up to 100 MeV the HVL can have (10 cm). In many areas such as A and B the FeSO_4 can reach good values than other compounds.

For the energy range 0.01 up to 100 MeV the photon attenuation coefficient for the samples record the overlapping values while the MFP record (1-10 cm) for the interesting energy region (0.1-100 MeV) as shown in Fig. 11.

For proton and alpha charge particles, the stopping power was calculated for the introduced compounds as shown in Fig. 12. Calculations were done using SRIM 2008.04 contributions supported freely by E. Dabich and J. F. Ziegler *et al.* 1984-2008. For proton, the compounds CuSO_4 and FeSO_4 have a peak value at 0.08 MeV while for Ni and Zn sulphate the maximum value is seen at 1 MeV proton energy. The situation is different for the alpha projectile it has stopping power peak at 0.08 keV for all samples.

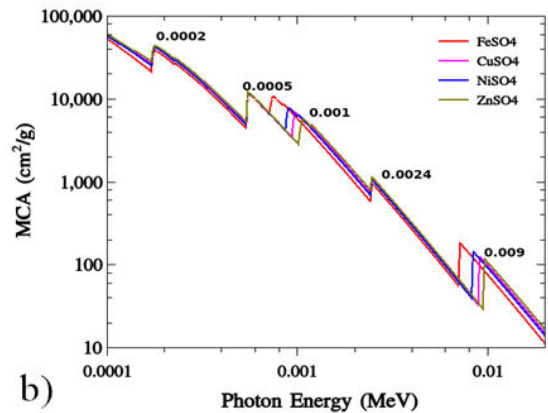
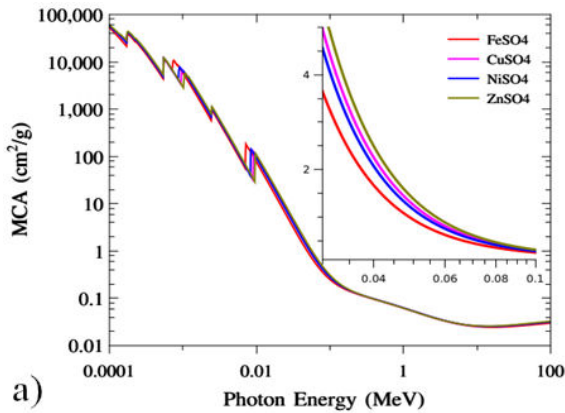


FIGURE 9. MAC of the introduced samples the right figure represents the low energy part.

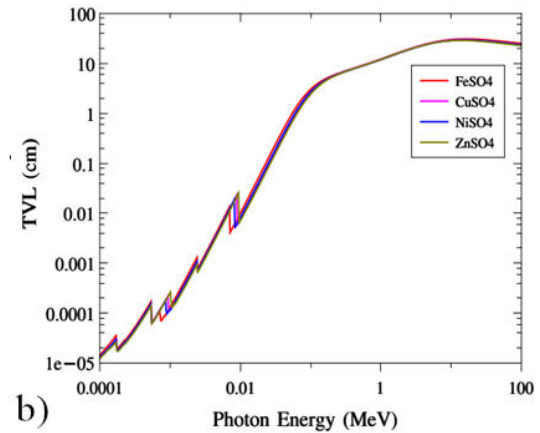
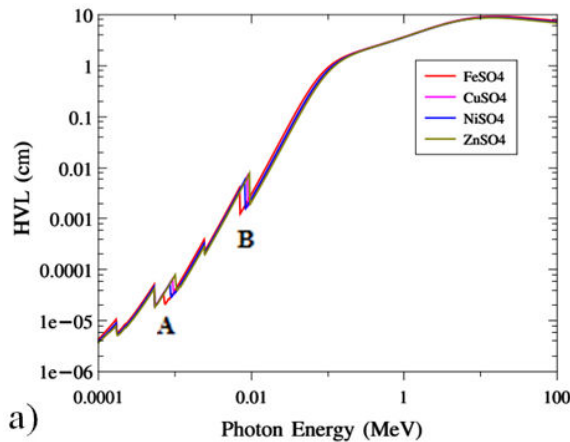


FIGURE 10. The HVL and the TVL for photon energy range (0.1 keV - 100 MeV).

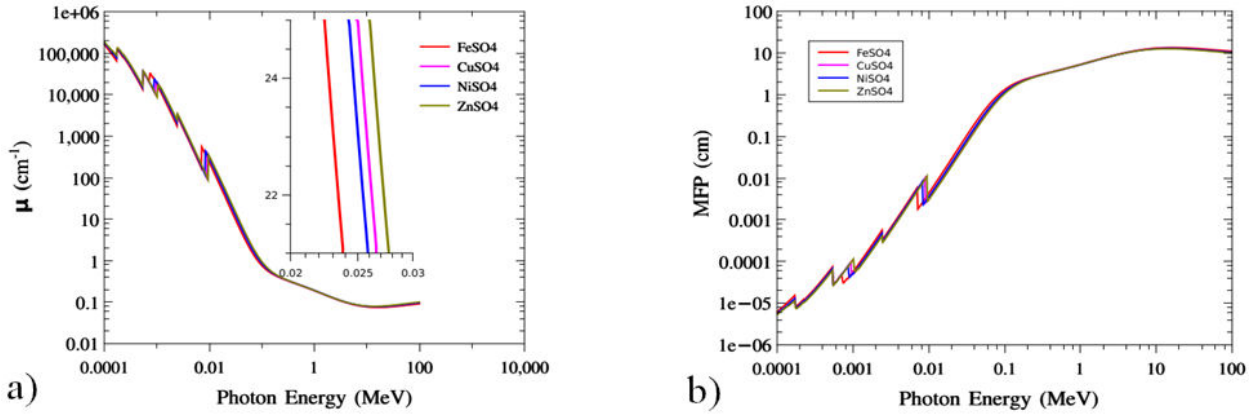


FIGURE 11. Represent the attenuation coefficient and mean free path for photon energy range up to 100 MeV.

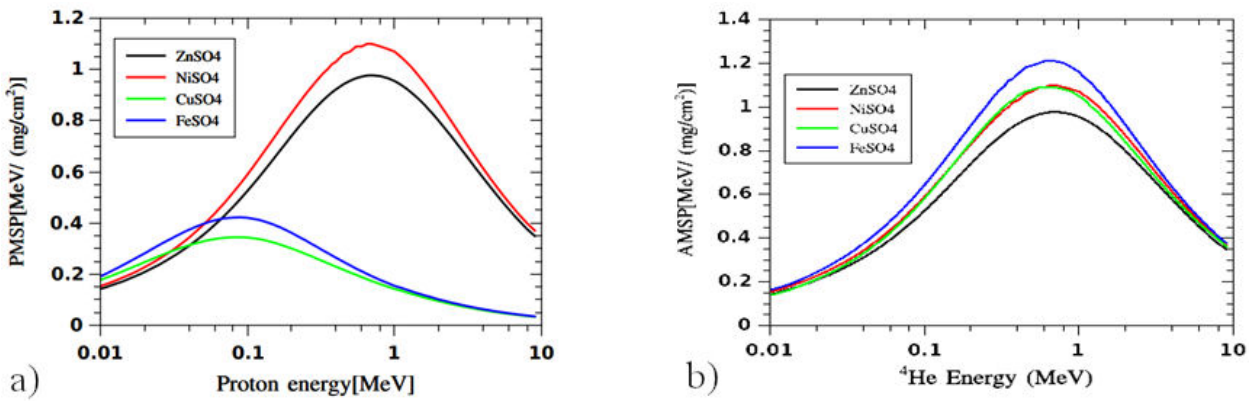


FIGURE 12. Represents the proton and alpha stopping power up to 10 MeV.

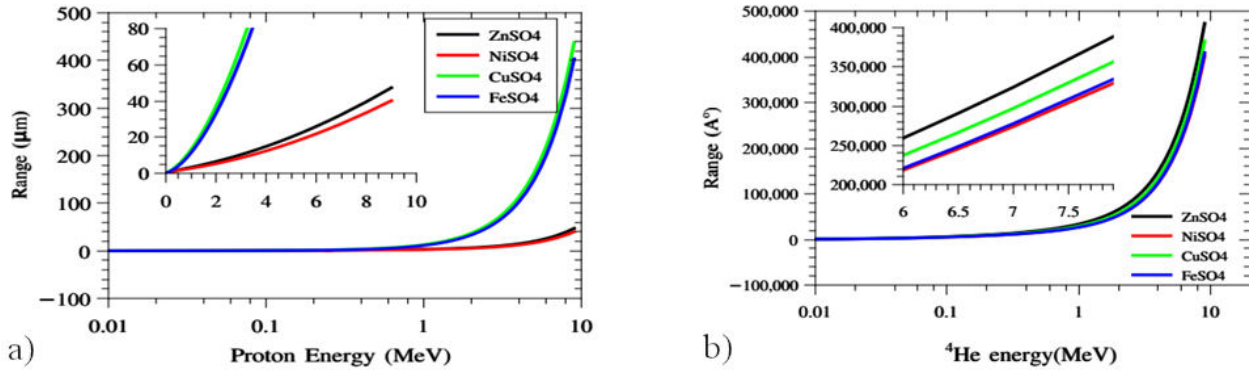


FIGURE 13. Represents the proton and alpha particle ranges for energy up to 10 MeV.

The proton and alpha 0.01-10 MeV ranges were calculated using the SRIM 2008.04 code Fig. 13. For proton, it is found that Cu and Fe have higher values than Zn and Ni sulphate but for the alpha particle range, Zn and Cu sulphate have the highest values than the other one.

Figure 14 shows a plot of Z_{eff} and Z_{eq} for the current samples in the range 0-15 MeV. Thus, the sample $FeSO_4$ possesses the lowest Z_{eff} and Z_{eq} because Fe has the lowest atomic weight 55.845 than other samples.

The thermal fast neutron effective removal cross-section (\sum_k in units of cm^{-1}) is revealed in the bar illustration for all samples in Fig. 15. In addition, the calculated $\sum R$ for the studied samples shows that S3 has the peaked value. Moreover, the lowest calculated value of $\sum R$ is for sample S4 has values of 0.25 and 0.096 cm^{-1} for thermal and fast neutron respectively.

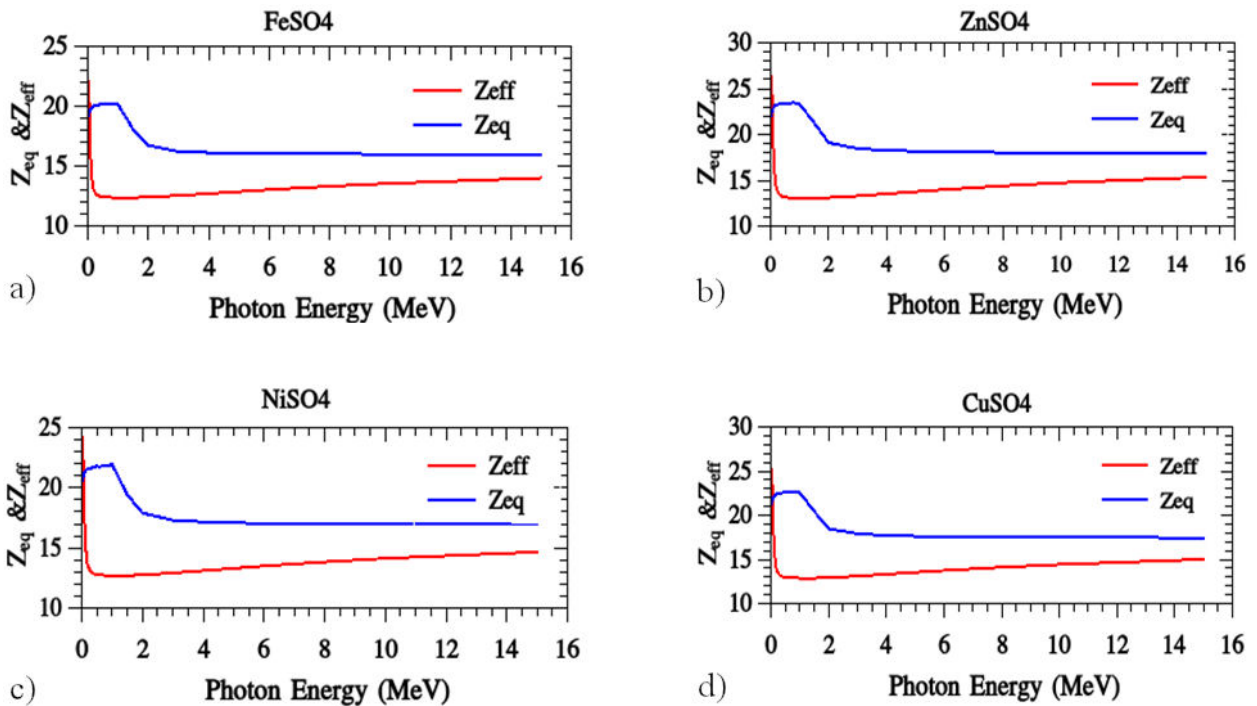


FIGURE 14. Represent the Z_{eff} and Z_{eq} of FeSO_4 , ZnSO_4 , NiSO_4 , and ZnSO_4 samples.

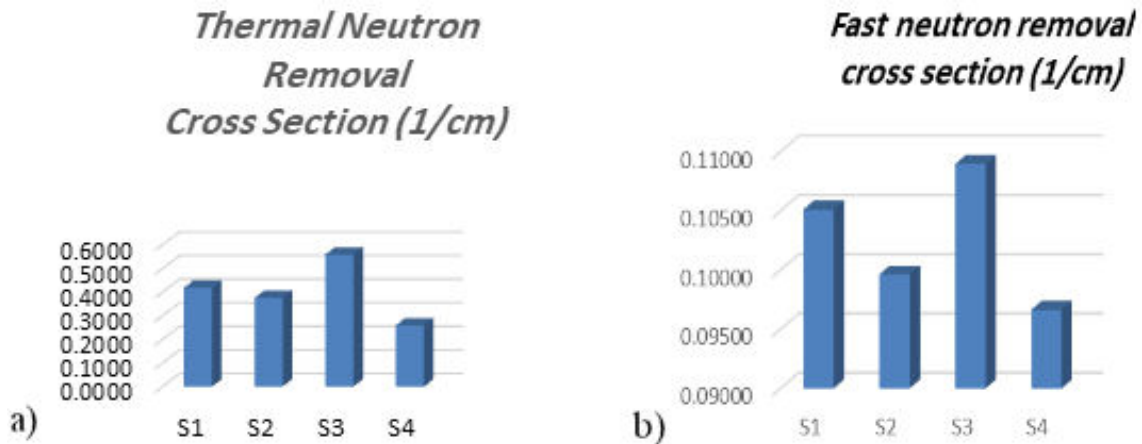


FIGURE 15. Fast and thermal neutron removal cross-section for S1-S4 Samples.

Conclusions

The full peak area for standard pure metals Fe, Cu, Ni, and Zn were calculated using the Origin 6.8 program. The accurate densities of such metals were well determined. Results show that these intensities reduced sharply for the selected sulphate compounds FeSO_4 , CuSO_4 , NiSO_4 and ZnSO_4 it should be mentioned that it is as low as possible when using iron sulphate. It is clear from the Scanning Electron Microscope SEM image investigation that, for Iron sulphate the granular shape of the surface particles and their distribution have a strong effect on the attenuation of X-rays, so the intensity decreased to less than 1000 compared to the metal one. The Monte Carlo using FLUKA code helps to know the wide

energy range of MCA. And the extracted other factors like (HVL) and (TVL) shows the trends of the studied samples to the incident photon radiations. Calculations for proton and alpha particles stopping power and ranges let us know CuSO_4 and FeSO_4 have a peak value at 0.08 MeV while for Ni and Zn sulphate the maximum value is seen at 1 MeV proton energy. In the case of the alpha projectile, it has a stopping power peak near 0.08 keV for all samples and the function has Gaussian trends than the proton particles. The calculation of the removal cross-section can explain that; the priority of the introduced samples can be arranged as S3, S1, S2, and S4 these arrangements are according to the heights of shielding efficiency for thermal and fast neutron modes.

Acknowledgment

We would like to thank Rajasthan University for all the technical support in completing the research

-
1. C. H. Holbrow *et al.*, Modern introductory physics (Springer, 2010).
 2. S. Gudennavar *et al.*, Verification of Bohr's frequency condition and Moseley's law: An undergraduate laboratory experiment, *American Journal of Physics* **71** (2003) 822.
 3. J. Gilfrich and L. Birks, Spectral distribution of X-ray tubes for quantitative X-ray fluorescence analysis, *Analytical chemistry* **40** (1968) 1077.
 4. S. Feldman, Nuclear weapons and arms control in the Middle East (MIT Press, 1997).
 5. T. Böhlen *et al.*, The FLUKA code: developments and challenges for high energy and medical applications, *Nuclear data sheets* **120** (2014) 211.
 6. A. B. Chilton, J. K. Shultis, and R. E. Faw, Principles of radiation shielding (1984).
 7. R. Cierniak, X-ray computed tomography in biomedical engineering (Springer Science & Business Media, 2011).
 8. B. Constantinescu *et al.*, Micro-SR-XRF and micro-PIXE studies for archaeological gold identification-The case of Carpathian (Transylvanian) gold and of Dacian bracelets, *Nuclear Instruments and Methods in Physics Research Section B: Beam Interactions with Materials and Atoms* **266** (2008) 2325.
 9. E. Sakar *et al.*, An extensive survey on radiation protection features of novel hafnium iron-borophosphate glasses: Experimental and theoretical study, *Progress in Nuclear Energy* **160** (2023) 104690.
 10. K. Janssens *et al.*, Use of microscopic XRF for non-destructive analysis in art and archaeometry, *X-Ray Spectrometry: An International Journal* **29** (2000) 73
 11. D. I. Tishkevich *et al.*, Effect of the synthesis conditions and microstructure for highly effective electron shields production based on Bi coatings, *ACS Applied Energy Materials* **1** (2018) 1695.
 12. M. F. Turhan *et al.*, A study for gamma-ray attenuation performances of barite filled polymer composites, *Applied Radiation and Isotopes* **191** (2023) 110568.
 13. J. E. Turner, Interaction of electrons with matter, Atoms, Radiation, and Radiation Protection (2007).
 14. V. Vlachoudis *et al.*, FLAIR: a powerful but user-friendly graphical interface for FLUKA, In Proc. Int. Conf. on Mathematics, *Computational Methods & Reactor Physics* (M&C 2009), Saratoga Springs, New York, **176** (2009).
 15. A. Fassò *et al.*, FLUKA: A Multi-particle Transport Code, CERN-2005-10, INFN/TC_05/11, SLAC-R-773 (2005).
 16. J. G. Adashko, The lexicon of Russian physics: a philological description (New York University, 1972).
 17. N. A. Alsaif *et al.*, Elastic-mechanical, dielectric properties, and γ -radiation safety competence of calcium boro-zinc glass systems reinforced with Nb⁵⁺ ions: experimental and theoretical studies, *Journal of Materials Science: Materials in Electronics* **34** (2023) 402.
 18. H. G. Özdemir *et al.*, Investigation of gamma radiation shielding characteristics of bismuth reinforced ternary composites in wide photon energy region, *Radiation Physics and Chemistry* **208** (2023) 110924.
 19. A. Von Bohlen, S. RÄ¶hrs, and J. Salomon, Spatially resolved element analysis of historical violin varnishes by use of μ PIXE, *Analytical and bioanalytical chemistry* **387** (2007) 781.
 20. E. Sakar *et al.*, Evaluation of γ -rays and neutron shielding parameters of high dense bismo-boro-tellurite glasses: comparative study, *Radiation Physics and Chemistry* **196** (2022) 110149.
 21. D. A. Aloraini *et al.*, Experimental and theoretical analysis of radiation shielding properties of strontium-borate-tellurite glasses, *Optical Materials* **121** (2021) 111589.
 22. A. El-Denglawey *et al.*, Prediction of mechanical and radiation parameters of glasses with high Bi₂O₃ concentration, *Results in Physics* **21** (2021) 103839.
 23. S. Huse *et al.*, Study on the radiation shielding features of some chemical compounds, In *Journal of Physics: Conference Series*, vol. 1644 (IOP Publishing, 2020) p. 012061.
 24. A. M. El-Khatib *et al.*, Fast and thermal neutrons attenuation through micro-sized and nano-sized CdO reinforced HDPE composites, *Radiation Physics and Chemistry* **180** (2021) 109245.
 25. F. Akman *et al.*, Gamma, charged particle and neutron radiation shielding capacities of ternary composites having polyester/barite/tungsten boride, *Radiation Physics and Chemistry* **212** (2023) 111120.